SCISSOR solitons and other novel propagation effects in microresonator-modified waveguides

John E. Heebner and Robert W. Boyd

Institute of Optics, University of Rochester, Rochester, New York 14627

Q-Han Park*

Department of Physics, Kyunghee University, Seoul, 130-701, Korea

We consider the linear and nonlinear optical properties of an optical waveguide consisting of a side-coupled integrated spaced sequence of resonators (SCISSOR). This fully transmissive system possesses large and controllable dispersion because the phase shift imparted by each resonator is strongly frequency dependent. Additionally, near resonance, the circulating power in each resonator can greatly exceed the power carried by the waveguide, leading to greatly enhanced nonlinear effects. We show that the effects of nonlinearity and dispersion can be balanced to create temporal solitons and that many other novel and useful pulse propagation effects can occur over short propagation distances in such a structure. © 2002 Optical Society of America

OCIS codes: 190.4390, 190.5530, 130.4310, 130.3120.

1. INTRODUCTION

A waveguide-coupled microdisk or microring resonator behaves much like a Gires–Tournois interferometer, which is simply a Fabry–Perot interferometer with a 100% reflecting back mirror. Such a configuration is simple and yet extremely interesting because it has the ability to modify the phase and enhance the circulating intensity through energy storage while possessing only one exit port through which unit transmission is sustained at all frequencies. Such a device is known as an all-pass or phase-only filter. Manufacturing techniques have progressed to the point where microdisk or microring resonators can be fabricated with circumferences corresponding to hundreds and even tens of optical wavelengths. This size corresponds to azimuthal mode spacings of the order of many terahertz, allowing for resonance bandwidths of the order of tens of gigahertz to terahertz. Because of these attractive features, microresonators have found application in disk lasers,[1–4] add–drop filters for wavelength-division multiplexing,[5] high-resolution spectroscopy,[6] laser frequency stabilization,[7] dispersion compensation,[8] all-optical switching,[9,10] and cavity quantum electrodynamics.[11] In this paper we describe how resonators can be used to tailor the linear and nonlinear pulse propagation characteristics of an ordinary dielectric waveguide. We begin with a review of basic relations that describe waveguide-coupled resonators and then proceed to describe pulse propagation effects for sequences of waveguide-coupled resonators.

2. RESONATOR BASICS

Figure 1 illustrates a sequence of waveguide-coupled resonators. The resonators are situated close to the waveguide to achieve evanescent coupling but are spaced far enough from one another that direct resonator-to-resonator coupling is negligible. First, we examine the basic relations among the incident ($\widetilde{E}_1$), transmitted ($\widetilde{E}_2$), and circulating ($\widetilde{E}_3$, $\widetilde{E}_4$) fields of a single resonator. In the spectral domain the fields exiting the coupling region are related to the input fields through the following unitary matrix:

$$\begin{bmatrix} \widetilde{E}_4(\omega) \\ \widetilde{E}_2(\omega) \end{bmatrix} = \begin{bmatrix} r & it \\ it & r \end{bmatrix} \begin{bmatrix} \widetilde{E}_3(\omega) \\ \widetilde{E}_1(\omega) \end{bmatrix}, \tag{1}$$

where the lumped self- and cross-coupling coefficients r and t are assumed to be independent of radian frequency (ω) and satisfy the relation $r^2 + t^2 = 1$. Propagation along the circumference ($2\pi R$) of the resonator may take the form of a mode of a ring waveguide or whispering-gallery mode[12] of a disk or sphere with effective index n_0. Along this feedback path, assuming attenuation and intrinsic dispersion are negligible, the field simply acquires an *internal* phase shift ϕ:

$$\widetilde{E}_3(\omega) = \exp[i\phi(\omega)]\widetilde{E}_4(\omega), \tag{2}$$

$$\phi(\omega) = 2\pi R n_0 \omega/c. \tag{3}$$

Solution of Eqs. (1) and (2) yields the following expressions for the transmitted $\widetilde{E}_2$ and circulating $\widetilde{E}_3$ steady-state monochromatic fields:
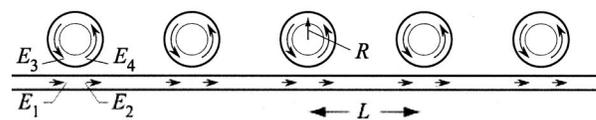
Fig. 1. Structured, fully transmissive waveguide and resonator configuration, forming a SCISSOR. E_1 is the incident field, E_4 is the field injected into the disk, E_3 is the field after one pass around the resonator, and E_2 is the transmitted field.
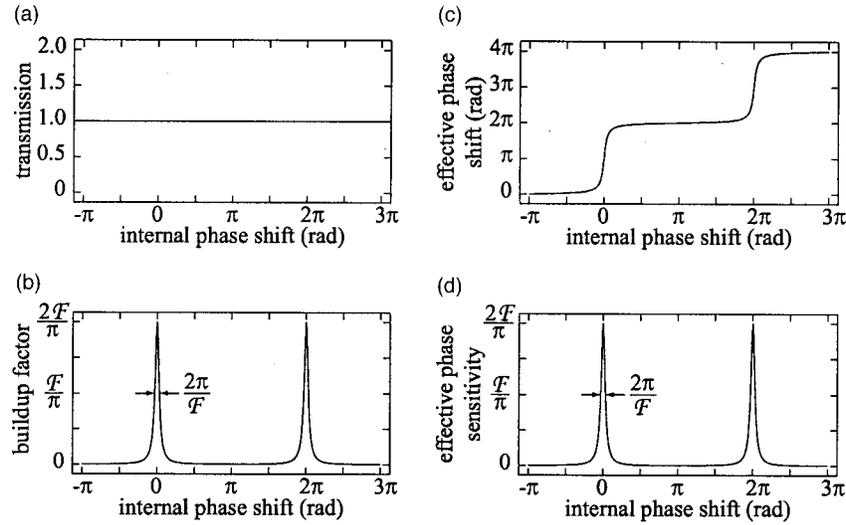
Fig. 2. (a) Transmission, (b) build-up factor, (c) effective phase shift acquired on transmission, and (d) phase sensitivity [derivative of (c)] plotted versus the internal phase shift for a waveguide-coupled resonator with a finesse of 10π.

$$\tilde{E}_2(\omega) = \frac{r - \exp[i\phi(\omega)]}{1 - r\exp[i\phi(\omega)]}\tilde{E}_1(\omega), \qquad (4)$$

$$\tilde{E}_3(\omega) = \frac{it\exp[i\phi(\omega)]}{1 - r\exp[i\phi(\omega)]}\tilde{E}_1(\omega). \qquad (5)$$

The transmission $|\tilde{E}_2/\tilde{E}_1|^2$ is equal to unity for all values of ω, and thus the field traversing the device simply acquires a *transmitted* phase shift Φ that exhibits the following frequency dependence:

$$\tilde{E}_2(\omega) = \exp[i\Phi(\omega)]\tilde{E}_1(\omega), \qquad (6)$$

$$\Phi(\omega) = \pi + \phi(\omega) + 2\arctan\frac{r\sin\phi(\omega)}{1 - r\cos\phi(\omega)}. \qquad (7)$$

Near resonance, the transmitted phase shift Φ becomes increasingly more sensitively dependent on the internal phase shift ϕ with increasing values of r. This increase in the slope of Φ versus ϕ is attained at the price of a slower response time. In addition to the increased phase sensitivity ($d\Phi/d\phi$), the circulating intensity becomes more intense in comparison with the incident intensity as a consequence of the coherent buildup of input power. This intensity enhancement or buildup factor is derived from Eq. (5) as

$$\mathcal{B}(\omega) = \left|\frac{\tilde{E}_3(\omega)}{\tilde{E}_1(\omega)}\right|^2$$

$$= \frac{1 - r^2}{1 - 2r\cos\phi(\omega) + r^2}$$

$$\xrightarrow[r\approx 1]{} \frac{\mathcal{B}_0}{1 + \mathcal{B}_0^2\sin^2[\phi(\omega)/2]}. \qquad (8)$$

Near resonance, the buildup factor is a sharply peaked function of the internal phase shift ϕ peaking at each integer multiple of 2π rad. The peak of the buildup factor, $\mathcal{B}_0 = (1 + r)/(1 - r)$, increases dramatically with r. A

convenient parameter characterizing the strength of the resonance is the finesse, which we define as the free spectral range (FSR) divided by the full width at half-depth of the resonance peak.[13] The finesse is related to the peak buildup factor as $\mathcal{F} \approx (\pi/2)\mathcal{B}_0$. The buildup factor and the phase sensitivity ($d\Phi/d\phi$) are equal for all ϕ. This is not a coincidence; rather, the result is a consequence of energy conservation: The increase in stored field energy results from an equivalent compression in time, which demands a lengthened response time. These fundamental characteristics of resonators are summarized graphically and plotted against the internal phase shift in Fig. 2.

3. LINEAR PROPAGATION EFFECTS

A pulse propagating though a single resonator acquires a frequency-dependent phase shift that serves to delay or distort the pulse shape. Arranging a sequence of resonators coupled to an ordinary waveguide can modify the effective propagation constant of the guide. The modified effective propagation constant can be defined as the accumulated phase per unit length and is composed of the propagation constant of the waveguide plus a contribution from the transmitted phase of the resonators. For a resonator spacing of L, the effective propagation constant becomes

$$k_0(\omega) = n_0\omega/c + \Phi(\omega)/L. \qquad (9)$$

A plot of the dispersion relation (propagation constant versus radian frequency) for various values of the coupling parameter r is shown in Fig. 3. The deviation in the curve from a straight line for an ordinary (dispersionless) waveguide will lead to periodic changes in the group velocity and group-velocity dispersion (GVD) with a periodicity of c/n_0R.

A pulsed waveform can be decomposed into the product of a slowly varying envelope $A(t)$ and a carrier wave with frequency ω_0 as $E(t) \equiv \frac{1}{2}A(t)\exp[ik_{\text{eff}}(\omega_0)z - i\omega_0t] + \text{c.c.}$ The relationship of the carrier frequency to some resonance frequency sets the central operating point on the dispersion relation curve and thus prompts the definition
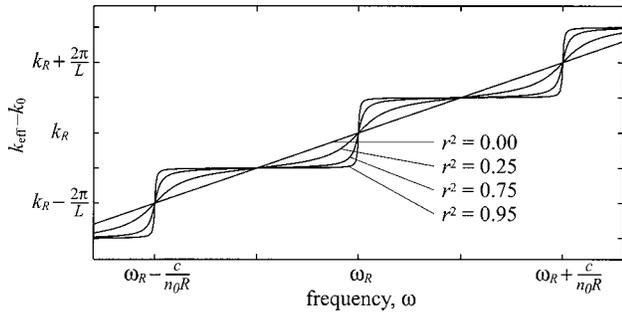
Fig. 3. Dispersion relation (propagation constant versus frequency) for light propagation in a SCISSOR with differing values of the self-coupling coefficient r. For generality, the waveguide contribution of constant slope k_0 has been subtracted from the effective propagation constant k_{eff}.

of a normalized detuning (actually, the internal phase shift of the carrier wave) $\phi_0 = (\omega_0 - \omega_R)T_R$, where T_R = FSR^{-1} is the resonator transit time and ω_R is the closest resonance frequency. The transfer function of a single resonator can be expanded in two embedded Taylor's series, one for the transmitted phase shift (expanded about the normalized detuning ϕ_0), and one for the exponential (expanded about the transmitted phase shift of the carrier Φ_0):

$$
H(\omega) = \exp(i\Phi)
$$
$$
= \exp(i\Phi_0)\left\{ 1 + \sum_{n=1}^{\infty} \frac{i^n}{n!}\left[\sum_{m=1}^{\infty} \frac{1}{m!} \frac{\mathrm{d}^m\Phi}{\mathrm{d}\phi^m}\bigg|_{\phi_0} \right.\right.
$$
$$
\left.\left. \times (\phi - \phi_0)^m \right]^n \right\}. \tag{10}
$$

Using this formal expansion, we relate the transmitted field to the incident field and make the assumption that the transmitted phase shift induced by each resonator is distributed over the spacing L so that the effective propagation constant is independent of propagation distance at the macroscopic scale. The field at some point z_{j+1} separated an infinitesimally small distance δz from the field at another z_j is given by a similar equation that distributes the resonator contribution and includes that of the waveguide:

$$
\bar{E}_{j+1}(\omega) = \exp\left[i\left(\frac{n_0\omega_0}{c} + \frac{\Phi_0}{L} \right)\delta z \right]\left\{ 1 + \sum_{n=1}^{\infty} \frac{i^n}{n!}\left[\frac{n_0}{c}\Delta\omega\delta z \right.\right.
$$
$$
\left.\left. + \sum_{m=1}^{\infty} \frac{1}{m!} \frac{\delta z}{L} \frac{\mathrm{d}^m\Phi}{\mathrm{d}\phi^m}\bigg|_{\phi_0} (\phi - \phi_0)^m \right]^n \right\}\bar{E}_j(\omega). \tag{11}
$$

Taking the Fourier transform of this equation results in a difference equation relating the pulse envelopes at the two points:

$$
A_{j+1}(t) = A_j(t) + \sum_{n=1}^{\infty} \frac{i^n}{n!}\left[i\frac{n_0}{c}\delta z\frac{\partial}{\partial t} \right.
$$
$$
\left. + \sum_{m=1}^{\infty} \frac{1}{m!} \frac{\delta z}{L} \frac{\mathrm{d}^m\Phi}{\mathrm{d}\omega^m}\bigg|_{\phi_0} \left(iT_R\frac{\partial}{\partial t} \right)^m \right]^n A_j(t). \tag{12}
$$

Finally, we make the differential approximation $[A_{j+1}(t) - A_j(t)]/\delta z \rightarrow \mathrm{d}A/\mathrm{d}z$ and allow δz to go to zero.[14] This procedure yields a linear propagation equation for the pulse envelope:

$$
\frac{\mathrm{d}A}{\mathrm{d}z} = \left[-\frac{n_0}{c}\frac{\partial}{\partial t} + i\sum_{m=1}^{\infty} \frac{1}{m!} \frac{1}{L} \frac{\mathrm{d}^m\Phi}{\mathrm{d}\omega^m}\bigg|_{\phi_0} \left(iT_R\frac{\partial}{\partial t} \right)^m \right]A. \tag{13}
$$

We isolate and examine the different terms in this equation in what follows.

A. Group-Velocity Reduction
The increased phase sensitivity on resonance is related to an increased group delay per resonator. This extra delay distributed amongst the resonators is responsible for a slower group velocity. The inverse of the group velocity is proportional to the frequency derivative of the propagation constant,

$$
k'_{\text{eff}} = \frac{\mathrm{d}k_{\text{eff}}}{\mathrm{d}\omega} = \frac{n_0}{c} + \frac{1}{L}\frac{\mathrm{d}\Phi}{\mathrm{d}\omega}
$$
$$
= \frac{n_0}{c}\left[1 + \frac{2\pi R}{L}\left(\frac{1 - r^2}{1 - 2r\cos\phi_0 + r^2} \right) \right]
$$
$$
\xrightarrow[\phi_0=0,r\approx1]{} \frac{n_0}{c}\left(1 + \frac{4R}{L}\mathcal{F} \right). \tag{14}
$$

The group velocity $1/k'_{\text{eff}}$ is seen to be composed of contributions from propagation in the waveguide and discrete delays introduced by the resonators. The component of the group-velocity reduction that is introduced by the resonators is proportional to the finesse and can dominate the waveguide component for moderate values of the finesse.

B. Group-Velocity Dispersion
While propagation in the waveguide itself is assumed to be dispersionless, strong dispersive effects are induced by the resonator contribution. The GVD is proportional to the second frequency derivative of the effective propagation constant,

$$
k''_{\text{eff}} = \frac{\mathrm{d}k^2_{\text{eff}}}{\mathrm{d}\omega^2} = \frac{1}{L}\frac{\mathrm{d}^2\Phi}{\mathrm{d}\omega^2} = \frac{T_R^2}{L}\frac{-2r(1 - r^2)\sin\phi_0}{(1 - 2r\cos\phi_0 + r^2)^2}
$$
$$
\xrightarrow[\phi_0=\pm\pi\mathcal{F}\sqrt{3}]{} \mp\frac{3\sqrt{3}\,\mathcal{F}^2 T_R^2}{4\pi^2 L}. \tag{15}
$$

While the GVD coefficient is zero on resonance, appreciably strong normal (positive) or anomalous (negative) values of the dispersion can be obtained on the red (lower) or blue (higher) side of resonance. The dispersion maxima occur at detunings $\phi_0 = \pm\pi/\mathcal{F}\sqrt{3}$, where the magnitude of the GVD is proportional to the square of the finesse. This induced structural dispersion can be many orders of magnitude greater than the material dispersion of typical optical materials.[15] For example, a 10-ps optical pulse propagating in a sequence of resonators with a finesse of 10π, FSR of 10 terahertz (~5 μm diameter), and a spacing of 10 μm experiences a GVD coefficient k''_{eff} of roughly
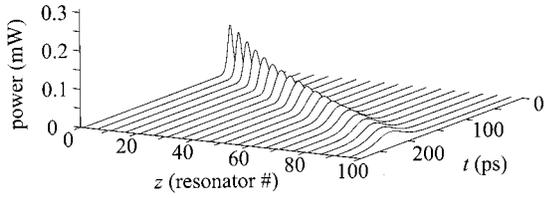
Fig. 4. A weak pulse tuned to the dispersion maxima disperses while propagating in a SCISSOR. A 10-ps FWHM hyperbolic secant pulse tuned for maximum anomalous GVD ($B = 0.13$) enters the system consisting of 100 resonators each with a 5-μm diameter and finesse of 10π, spaced by 10 μm. Note that the peak power is reduced by a factor of ~4 after propagating only 1 mm as a consequence of the strong induced dispersion.

100 ps^2/mm. In general, this structural dispersion can be as much as 7 orders of magnitude greater than material dispersion in conventional materials such as silica fiber (20 ps^2/km). Figure 4 shows the pulse evolution for a 10-ps pulse propagating through 100 resonators, each tuned to the anomalous dispersion maximum.

C. Higher-Order Dispersion

Higher orders of dispersion may be derived from Eq. (13), each subsequently possessing a maximum that is proportional to the cavity lifetime $\mathcal{F}T_R$ to the nth power. Specifically, the third-order dispersion coefficient is

$$
\begin{aligned}
k'''_{\text{eff}} &\equiv \frac{1}{L}\frac{d^3\Phi}{d\omega^3} \\
&= \frac{T_R^3}{L}\frac{-2r(1-r^2)[(1+r^2)\cos\phi_0 - 3r + r\cos 2\phi_0]}{(1 - 2r\cos\phi_0 + r^2)^3} \\
&\xrightarrow[\phi_0 = 0, r\approx 1]{} -\frac{4}{\pi^3}\frac{\mathcal{F}^3 T_R^3}{L}.
\end{aligned}
\tag{16}
$$

It is important to note that all orders of dispersion become significant when the pulse bandwidth is nearly as wide as the resonance bandwidth.

4. NONLINEAR PROPAGATION EFFECTS

A. Nonlinear Phase Shift

In addition to inducing a strong group delay and dispersion, a resonator may enhance a weak nonlinearity. If the resonator possesses a nonlinear refractive index, i.e., Kerr nonlinearity, then the internal phase shift will be intensity dependent. For simplicity we neglect the nonlinearity of the waveguide in what follows, since it is expected to be small. The intensity-dependent contribution of the resonators to the internal phase shift is given by $\gamma 2\pi R|\tilde{E}_3|^2$, where γ represents the strength of the intrinsic nonlinear propagation constant. This parameter is, of course, traditionally fixed for a given material system and can be as low as 0.002 m^{-1}W^{-1} for standard single-mode silica fiber or as high as 10^2 m^{-1}W^{-1} in an air-clad GaAs or chalcogenide-glass-based waveguide.[16] Near resonance, the transmitted phase shift is sensitively dependent on the internal phase shift, which is in turn dependent on an enhanced circulating intensity. The combined action of these effects gives rise to a dually enhanced ef-

fective nonlinear propagation constant γ_{eff}, calculated from the derivative of the transmitted phase shift with respect to the input intensity:

$$
\begin{aligned}
\gamma_{\text{eff}} &\equiv \frac{1}{L}\frac{d\Phi}{d|\tilde{E}_1|^2} \\
&= \frac{1}{L}\frac{d\Phi}{d\phi}\frac{d\phi}{d|\tilde{E}_3|^2}\frac{d|\tilde{E}_3|^2}{d|\tilde{E}_1|^2} \\
&= \frac{\gamma 2\pi R}{L}\left(\frac{1 - r^2}{1 - 2r\cos\phi_0 + r^2}\right)^2 \xrightarrow[\phi_0 = 0, r\approx 1]{} \gamma\frac{8R}{\pi L}\mathcal{F}^2.
\end{aligned}
\tag{17}
$$

As can be seen from this equation, the increased phase sensitivity (or group-velocity reduction) and the buildup of intensity contribute equally to quadratically enhance the nonlinear propagation constant with respect to the finesse.[17] To properly account for the all the third-order Kerr nonlinear contributions of the spectral components of three fields, a double convolution of the three interacting fields is performed in the spectral domain. In the time domain the double convolution operation is equivalent to multiplication. This allows for the straightforward addition of a nonlinear contribution[18] to the internal phase shift term in the linear propagation equation [Eq. (13)]:

$$
\begin{aligned}
\frac{dA}{dz} &= \left\{ -\frac{n_0}{c}\frac{\partial}{\partial t} + i\sum_{m=1}^{\infty}\frac{1}{m!}\frac{1}{L}\frac{d^m\Phi}{d\phi^m}\Bigg|_{\phi_0} \right. \\
&\quad \left. \times \left(\gamma 2\pi R\mathcal{B}|A|^2 + iT_R\frac{\partial}{\partial t}\right)^m \right\}A.
\end{aligned}
\tag{18}
$$

For two nonlinearly interacting resonant pulses, the results derived here for the self-phase modulation (SPM) effect apply to the cross-phase modulation effect equivalently.

B. Solitons

We next examine the nonlinear propagation equation that retains only the lowest-order dispersive and nonlinear terms in Eq. (18) and shift the time coordinate to the reference frame of the pulse ($\tau = t - k'_{\text{eff}}z$). We find that, in this limit, the pulse evolution is governed by a nonlinear Schrödinger equation with effective GVD and SPM parameters:

$$
\frac{\partial}{\partial z}A = -i\frac{1}{2}k''_{\text{eff}}\frac{\partial^2}{\partial\tau^2}A + i\gamma_{\text{eff}}|A|^2A.
\tag{19}
$$

Soliton solutions exist provided that the enhanced nonlinearity and induced dispersion are of opposite signs. While the sign of the enhanced nonlinearity is predetermined by the sign of the intrinsic nonlinearity, the sign of the induced dispersion is, as was previously shown in Eq. (15), determined by the sign of the normalized detuning from resonance. The fundamental soliton solution for this equation is

$$
A(z, \tau) = A_0 \,\text{sech}(\tau/T_P)\exp(i\tfrac{1}{2}\gamma_{\text{eff}}|A_0|^2 z),
\tag{20}
$$

where the amplitude and pulse width are related according to $|A_0|^2 = |k''_{\text{eff}}|/\gamma_{\text{eff}}T_P^2$, below which the pulse is severely distorted by all orders of dispersion. The finite response time of the resonator places a lower bound on the
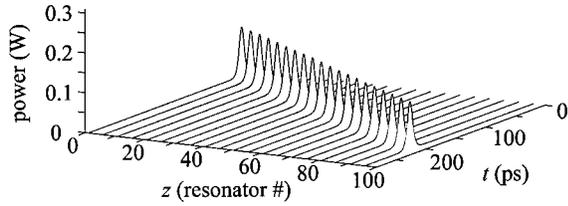
Fig. 5. A pulse with amplitude corresponding to the fundamental soliton propagates in a SCISSOR without dispersing. The same parameters were used as in Fig. 4, but with a peak power of 125 mW ($\Gamma = 0.0196$) in a chalcogenide-glass-based system.
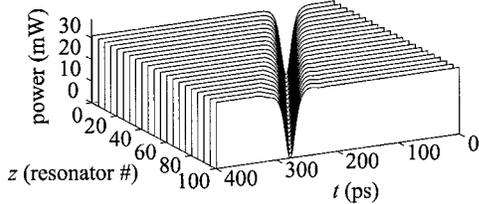
Fig. 6. A negative pulse in a uniform intensity background with parameters corresponding to the fundamental dark soliton propagates in a SCISSOR without dispersing. The incident field distribution was a hyperbolic tangent with twice the pulse width of the bright soliton and a background power that was one fourth that of its peak power in Fig. 5.

pulsewidth T_P. We define a scaling factor B to be the ratio of the pulse bandwidth $[2 \operatorname{arcsech}(1/\sqrt{2})/\pi^2 T_P]$ to the resonator bandwidth $(1/\mathcal{F}T_R)$, such that $B = [2 \operatorname{arcsech}(1/\sqrt{2})/\pi^2]\mathcal{F}T_R/T_P$. We also define a nonlinear strength parameter as $\Gamma = (4/\pi^2)\mathcal{F}^2\gamma|A_0|^2 R$. With these definitions a simple relation holds between Γ and B for the fundamental soliton operating at the anomalous dispersion peak[19]:

$$\Gamma = \frac{\pi}{2\sqrt{3}\operatorname{arcsech}^2(1/\sqrt{2})}B^2 \approx B^2. \qquad (21)$$

Higher-order dispersive and nonlinear terms become increasingly significant when either B or Γ approach unity.

To test the validity of this approximation, we have conducted rigorous time-domain simulations[20] in an attempt to propagate solitons. In Fig. 4 we showed the pulse evolution of a low-power 10-ps FWHM hyperbolic secant pulse tuned for maximum anomalous GVD ($B = 0.13$) in a chalcogenide-glass-based system. The system consisted of 100 resonators spaced by 10 μm each with a 5-μm diameter and finesse of 10π. As can be seen, the temporal pulse profile is greatly dispersed. Figure 5 shows the pulse evolution for the same system but with a peak power of 125 mW, corresponding to the fundamental side-coupled integrated spaced sequence of resonators (SCISSOR) soliton ($\Gamma = 0.0196$). As can be seen, the pulse shape is well preserved on propagation. Many of the familiar characteristics of fundamental solitons such as robustness, reshaping, pulse compression, and pulse expansion have been observed in simulations to carry over from the continuous-medium case. Higher-order solitons, satisfying $\Gamma \approx N^2 B^2$, where N is an integer, are readily observed in simulations but are unstable because of higher-order dispersive nonlinear effects present in this system.[21] We return to this point in the Subsection 4.C.

Dark solitons that consist of an intensity dip in an otherwise uniform continuous-wave field can also be supported if the enhanced nonlinearity and induced dispersion are of the same sign (on the other side of resonance). Figure 6 shows the propagation of the fundamental dark SCISSOR soliton (a hyperbolic tangent field distribution) tuned to the normal dispersion peak.

C. Self-Steepening

In Subsection 4.B we neglected the frequency dependence of γ_{eff}. One of the effects resulting from the frequency-dependent nature of γ_{eff} is an intensity-dependent group velocity. This effect leads to the phenomenon of self-steepening (SS) of a pulse, where the peak of a pulse travels slower than ($+$SS) or faster than ($-$SS) its wings. The SS coefficient s may be derived[22] from Eq. (18), but it is more readily obtained from the frequency derivative of the nonlinear coefficient:

$$s = \frac{\gamma'_{\text{eff}}}{\gamma_{\text{eff}}} = \frac{2}{\mathcal{B}}\frac{d\mathcal{B}}{d\omega}\xrightarrow[\phi_0 = \pm\pi/\mathcal{F}\sqrt{3}]{} \mp \frac{\sqrt{3}\mathcal{F}T_R}{\pi}. \qquad (22)$$

While it is difficult to isolate this effect from induced GVD in a sequence of resonators (see Fig. 11 below) to form a steepened pulse, it plays an important role in the breakup of higher-order solitons. The known phenomenon of soliton decay[18] involves the breakup of an Nth-order breathing soliton into N fundamental solitons of differing pulse amplitudes and widths. Figure 7 shows a situation in which a second-order SCISSOR soliton with a launched peak power of 500 mW undergoes decay and splits into two stable fundamental SCISSOR solitons. The solitons are well isolated in time and uncorrupted by a background or pedestal. One of them possesses a higher peak power and narrower width than the original, demonstrating the potential for pedestal-free optical pulse compression. The effects of induced SS in a sequence of resonators can take place for picosecond and even nanosecond pulses because, unlike in the case of intrinsic SS, the relative strength of SS to SPM is not governed by how close the pulse width is to being a single optical cycle, $2\pi/\omega_0$, but rather how close the pulse width is to being a single cavity lifetime $\mathcal{F}T_R$. For the 10-ps pulse propagating in a SCISSOR with the above parameters, the nondimensional SS parameter (S/T_P) is 0.173. In order to observe the same effect with traditional intrinsic SS, a 30-fs pulse would be required.
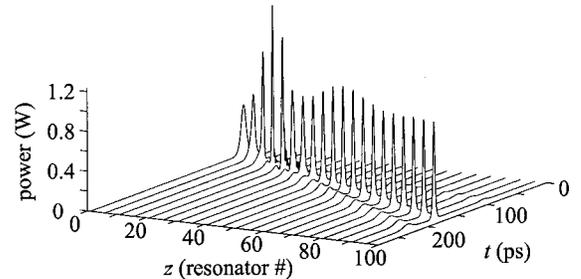
Fig. 7. A higher-order breathing soliton is unstable under the influence of the resonator-induced intensity-dependent group velocity (SS). Here a second-order soliton splits into two stable fundamental solitons on propagation in a SCISSOR. The incident field distribution was the same as in Fig. 5 but with four times the peak power.

D. Multistability and Saturation

In the previous section we added the SS correction to the nonlinear coefficient that resulted from the frequency dependence of γ_{eff}. Relation (17) was implicitly derived with the assumption of low intensity; now we examine the intensity dependence of γ_{eff} and find that the circulating intensity and γ_{eff} are in fact interdependent. The circulating intensity depends on the buildup factor, which in turn depends on the circulating intensity from the nonlinear detuning contribution. As a result nonlinear resonators can possess memory and multistable branches in the input–output relationships within certain operating regimes.[23] When operated near resonance, the onset of multistability occurs when the circulating power is high enough to generate a single-pass nonlinear phase shift of 2π rad. Saturation resulting from intensity-dependent detuning's pulling the resonator off resonance generally takes place well before this effect. Working on the lower branch of the multistable relation for positive detunings, we find that the saturation of the effective nonlinear propagation constant is well fitted by a $(1 + I/I_s)^{-1}$ type of saturation model, which is given explicitly as

$$\gamma_{\text{eff}}(|A|^2) \xrightarrow[r \approx 1]{} \frac{\gamma \dfrac{2\pi R}{L} \mathcal{B}_{\phi_0}^2}{1 + \dfrac{\gamma 2\pi R \mathcal{B}_{\phi_0}^2}{2\pi - \Phi_0}|A|^2}, \tag{23}$$

where the saturating intensity near resonance is $|A_S|^2 = \pi/\gamma_{\text{eff}}L$. The saturating intensity is lower for higher detunings from resonance. A generalized nonlinear Schrödinger equation incorporating every effect discussed so far takes the following form:

$$\frac{\partial}{\partial z}A + k'_{\text{eff}}\frac{\partial}{\partial t}A = -i\frac{1}{2}k''_{\text{eff}}\frac{\partial^2}{\partial t^2}A + \frac{1}{6}k'''_{\text{eff}}\frac{\partial^3}{\partial t^3}A$$
$$+ i\left(1 + is\frac{\partial}{\partial t}\right)\frac{\gamma_{\text{eff}}|A|^2}{1 + |A|^2/|A_S|^2}A. \tag{24}$$

E. Nonlinear Frequency Mixing

The characteristics of frequency mixing processes such as harmonic generation and four-wave mixing can also be enhanced by waveguide-coupled resonators. As a general rule, the scaling of the enhancement of these processes can be inferred by including contributions from each intensity involved (lying within a resonance) and the interaction length. Each contributes a factor proportional to the finesse.

Four-wave mixing is a third-order nonlinear process that annihilates two photons at one frequency and generates two photons at higher and lower frequencies. Four-wave mixing can give rise to modulation instability whereby a low-contrast amplitude ripple grows by the amplification of sidebands at the expense of the central frequency. In a dispersive medium, four-wave mixing is stifled owing to phase mismatch. However, in an anomalous dispersive medium positive SPM generates new frequency components that compensate for the mismatch.[18] If the process is allowed to continue, the modulation
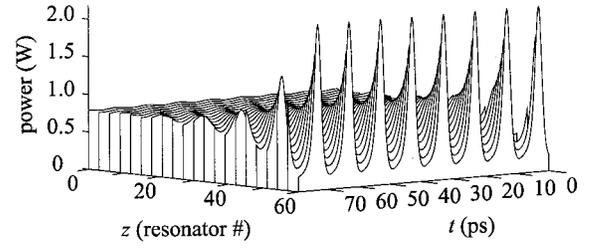
Fig. 8. Demonstration of modulation instability in a SCISSOR. The input field consists of 800 mW of cw power with a 1% power ripple. The SCISSOR parameters are chosen such that the peak of the instability gain is at the input modulation frequency of 100 GHz. Note that the modulation frequency given by Eq. (25) need not be a resonance frequency of the structure.

depth increases until a train of solitons stabilizes. Figure 8 shows the increase in modulation depth for a seeded 1% amplitude ripple of 100 GHz with propagation distance for a sequence of 60 resonators. The peak of the effective instability gain, $g_m = 2\gamma_{\text{eff}}|A_0|^2$, occurs at some modulation frequency

$$\Omega_m = \pm\sqrt{2\gamma_{\text{eff}}|A_0|^2/|k''_{\text{eff}}|}, \tag{25}$$

provided that this value does not exceed the resonance bandwidth. The gain is enhanced by the square of the finesse.

Until this point we have restricted our attention to pulses whose bandwidth is of the order or less than that of a single resonance peak. Copropagating pulses with carrier frequencies lying within differing resonance peaks can enhance four-wave mixing processes with frequency separations of pump and signal equal to an integer number of FSRs. Because the efficiency of idler generation depends on the pump intensity and signal intensity, and grows quadratically with length, the efficiency scales as the fourth power of the finesse.[24] We expect such effects to be important in systems that have low intrinsic dispersion such that the FSR is independent of frequency so that the three enhancement linewidths coincide with signal, pump, and idler frequencies. Finally, the efficiency of harmonic generation processes may be increased.[25] The efficiency of second-harmonic generation, for example, would be enhanced cubically with the finesse.

5. FURTHER IMPLICATIONS

A. Attenuation

Until this section we have assumed that loss is negligible; here we return to examine the effects of attenuation on the performance of microdisk phenomena. Attenuation in microesonators is in general detrimental. Internal attenuation reduces the net transmission, buildup, and (in general) the nonlinear response. It also broadens the resonance limiting the achievable finesse.[26] Attenuation in microresonators typically arises from three mechanisms: intrinsic absorption, radiation loss,[27] and scattering. Intrinsic absorption can typically be rendered insignificant over millimeter-sized propagation distances by choosing an appropriate material system at a given wavelength. Additionally, since the circulating intensity can greatly exceed the incident intensity, intensity-dependent absorption processes such as two-

photon absorption may be significant in resonators. Two-photon absorption may be minimized by proper selection of a material with a bandgap that is greater than twice the incident photon energy.[28] Whispering-gallery modes of a disk and modes of a ring waveguide suffer from bending or radiation loss, which is increasingly important for small resonators with low refractive-index contrast. Figure 9 plots the radiation-loss-limited finesse of a free uncoupled resonator versus the normalized radius for various refractive-index contrasts. Scattering can take place in the bulk or on the surfaces. Surface scattering is typically the dominant loss mechanism and results from roughness on the microresonator edges, which in practice cannot be made perfectly smooth.[29] The surface perturbations phase match the guided mode to radiating modes. Figure 10(a) shows a finite-difference time-domain[30] simulation of a five-resonator SCISSOR with 50-nm sidewall roughness, displaying strong scattering losses and weak circulating intensity. In Fig. 10(b) a lower sidewall roughness of 30 nm results in negligible scattering loss and strong-intensity buildup.

Resonators have the ability to modify and in some cases enhance certain figures of merit. A common figure of merit is the ratio of the nonlinear coefficient to the linear absorption. While the nonlinear coefficient is quadratically dependent on the finesse, the linear absorption, much like the group-velocity reduction, exhibits only a linear proportionality. As a result, the figure of merit is enhanced proportional to the finesse.[31] Gain may be implemented where possible to combat attenuation. More interestingly, a dispersion-decreasing system may be used to propagate a SCISSOR soliton in an attenuating structure. In this case the pulse width is kept constant as the amplitude decreases by means of an exponential decrease in dispersion down the length of the structure.

B. Phase Depth

Within a FSR, a *single* resonator can impart only a maximum phase depth of 2π rad. This limitation has important implications for the maximum delay and chirp and the nonlinear phase that can be imposed on a pulse per resonator. As the imparted phase nears only $\pi/2$ rad, higher-order effects become increasingly significant such that the system can no longer be treated perturbatively. The extent of group-velocity reduction that can be
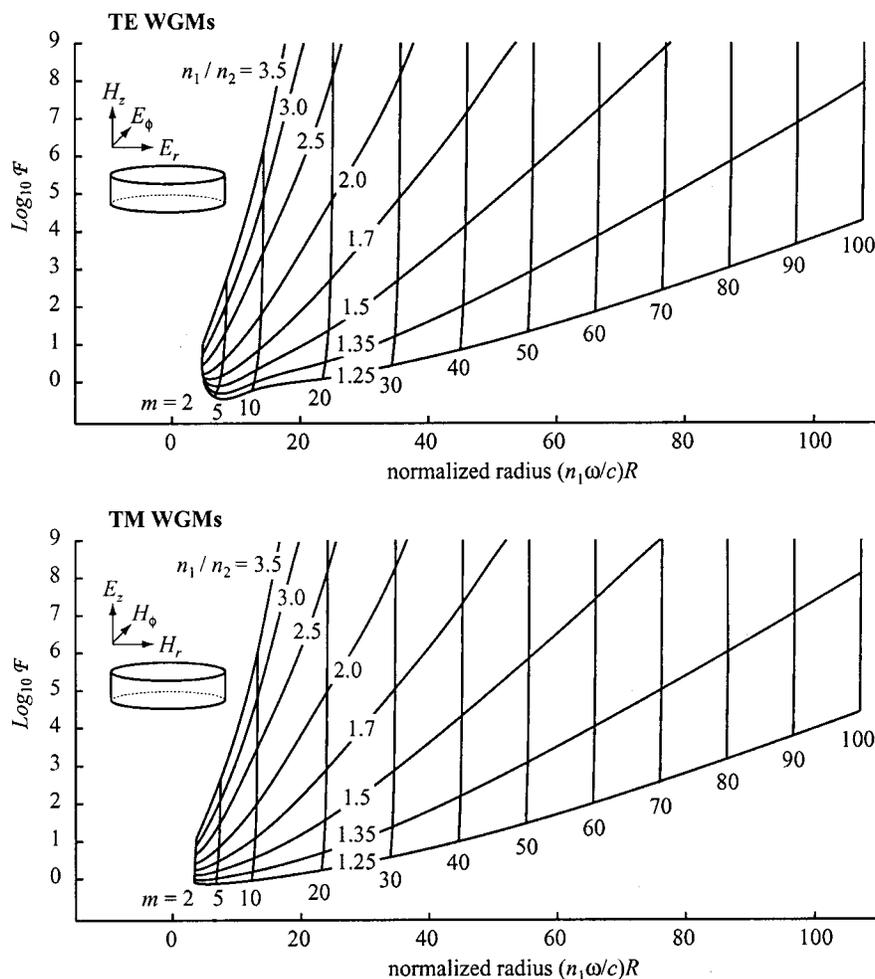
Fig. 9. Radiation-loss-limited finesse of the lowest-order radial TE and TM whispering-gallery modes of a dielectric cylinder of index n_1 in a medium of index n_2 plotted versus normalized radius $(n_1\omega/c)R$. The family of diagonal curves represents varying refractive-index contrasts (n_1/n_2). The family of nearly vertical curves corresponds to whispering-gallery mode resonances, each characterized by an azimuthal mode number m. The plots were obtained by numerical solution of the dispersion relation for whispering-gallery modes.
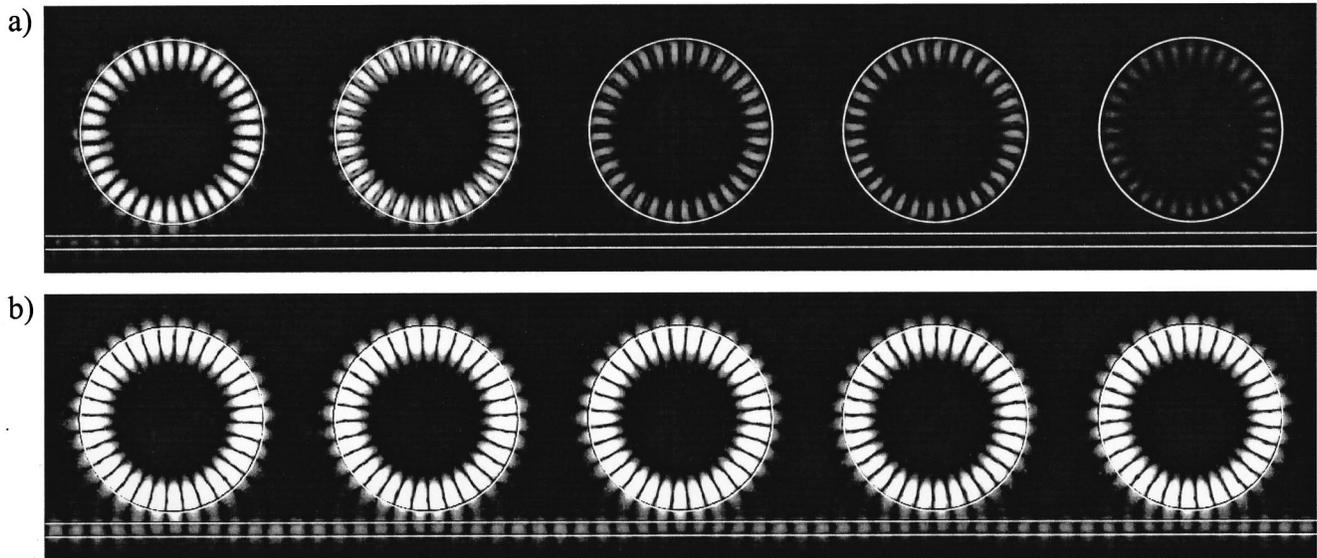
Fig. 10. Finite-difference time-domain method of solving Maxwell's equations for a SCISSOR structure composed of 5 microresonators. A TE field of wavelength 1.55 μm is launched into the 0.4-μm-wide waveguide evanescently side coupled to a disk with a diameter of 5.1 μm. The refractive index of the air-clad disk and guide is 2. Exclusive coupling to the $m = 16$ azimuthal whispering-gallery mode is achieved by careful selection of parameters. (a) Strong scattering losses result due to roughness associated with a 50 nm grid. (b) Scattering losses are made negligible by use of a 30-nm grid. Consequently, a buildup factor of 16 and finesse of 25 are achieved in this structure.

achieved in a SCISSOR is limited by how high the finesse can be made. A SCISSOR with an ultrahigh value of finesse can be used to slow a pulse appreciably, but that pulse must be long enough that it is at least of the order of the finesse times the transit time of a single resonator. Thus the maximum delay per resonator is fixed and equal to one pulse width at best. The same is true for the induced GVD. A high GVD coefficient (proportional to $\mathcal{F}^2$) can be obtained if the finesse is made very large. However, the increasing finesse places an increasing restriction on the pulse bandwidth $\Delta\omega$ (proportional to $1/\mathcal{F}$). As a result, the imposed spectral chirp per resonator, $1/2k''_{\text{eff}}\Delta\omega^2L$, is independent of finesse and dependent only on the scaling factor B. If the requirement is to broaden a pulse by N pulse widths, then the minimum number of resonators needed (occurring at $B \sim 1$) is roughly N. This is an important point: an ultrahigh finesse is not required for designing dispersive devices based on resonators. However, while reducing the resonator size and increasing the finesse in inverse proportion maintains the same resonator bandwidth and thus the same linear properties, the nonlinear properties are enhanced. This is of fundamental importance, since a low threshold power and small number of resonators is desirable in practice. As a result of saturation, it is difficult to achieve an effective nonlinear phase shift of π rad from a single resonator when operating on resonance. It is achieved only in the limit as the resonator's internal phase shift is power detuned completely by π rad, resulting in an external phase shift of π rad as well. As a result of this saturation, one completely loses the advantage of resonant enhancement. A phase shift of $\pi/2$ is, however, much easier to attain before the saturation takes place and requires a power detuning of only $\phi = \pi/\mathcal{F}$. A nonlinear external phase shift of π may be readily obtained from a single resonator,

taking advantage of enhancement by ensuring that the resonator is initially red detuned by $\pi/\mathcal{F}$ and allowing the resonator to be power detuned through resonance for a total value of π rad. We expect these universal restrictions to be important in the design of SCISSOR systems and other photonic structures containing microresonators.

C. Analogous Systems
We now turn our attention to comparing and contrasting the geometry and propagation characteristics of our system with that of other well-known systems in optical physics.

In certain respects, the SCISSOR soliton is analogous to the gap[32] or more general Bragg[33] soliton, which results from nonlinear pulse propagation within or near the photonic bandgap of a distributed feedback structure. The SCISSOR structure itself bears some similarity to a coupled-resonator optical waveguide,[34] which consists of a two- or three-dimensional array of intercoupled resonators and no side-coupled waveguide. Because each constituent resonator of a SCISSOR is an all-pass filter, feedback is present within each resonator but not among resonators. Alternatively, there is no intended mechanism for light to couple into the counterpropagating modes of the microresonator or guide. As a result, there is no frequency at which light is restricted from propagating, and thus the structure does not possess a photonic bandgap. Nevertheless, the SCISSOR structure displays enhanced nonlinear optical response for much the same reason that a photonic bandgap structure can produce enhanced nonlinearity. Because of this, it is not necessary for the resonators to be periodically spaced: only the average density of resonators is important. The addition of a second guide on the other side of the resonator array, however, opens the possibility for interresonator feedback

and the existence of a photonic bandgap. This type of structure is interesting in its own right,[35] and its propagation characteristics will be reserved for separate investigation.[36]

Many properties of our system are analogous to those found in atomic systems. In both cases light is coupled into and out of discrete resonators without loss or dispersion but with delay. It is known from studies of slow light propagation in atomic systems displaying electromagnetically induced transparency that the width of the induced transparency window in atomic systems with N interacting atoms is reduced[37] by a factor that scales as $N^{-1/2}$. This fundamental limitation on bandwidth results from the fact that near the frequency of maximum transmission the transmission decreases quadratically with detuning. Such a limitation is absent in a fully transmissive SCISSOR geometry used to propagate solitons, but a fundamental limitation is imposed by fourth-order dispersion. A careful analysis shows that the bandwidth reduction in a SCISSOR structure with N interacting resonators scales much slower, as $N^{-1/4}$. A sequence of resonators might someday be useful in studying the properties of slow light in the regime where acoustic and optical group velocities are of the same order of magnitude.[38,39] To slow the group propagation to this level in silica, a finesse of $\sim 10^5$ is required.

6. CONCLUSION

Passive, nonlinear resonators are still a relatively largely untapped area of research. At present, many single-microresonator systems with excellent optical properties have been constructed.[40-44] In many of these cases, extending the fabrication techniques to construct long sequences of such devices to yield large-scale integration of photonic devices[45] is achievable. Additionally, it would also be possible to fabricate SCISSOR devices by coupling silica glass microsphere resonators to an optical waveguide. The modes of glass spheres have been shown to possess high values of finesse (10^5),[11] which could be useful in slow light applications. However, excercising precise control of the resonator diameter and coupling coefficient would be more difficult than for a SCISSOR formed by use of lithographic techniques. In this paper we have described some of the linear and nonlinear transfer characteristics of single microresonators and the propagation characteristics of sequences of microresonators. Figure
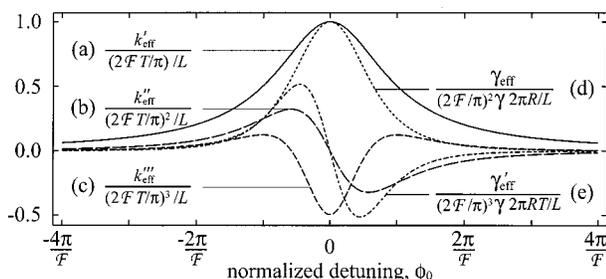
11 summarizes the main characteristics in a graphical manner as a function of detuning. The application of thermal or electrical fields to the resonators makes it possible to control the detuning or coupling coefficients. We envision that such structures could be used as artificial media to study and apply nonlinear Schrödinger equation pulse propagation effects on an integrated chip where the propagation parameters may be chosen or modified in real time. Other applications might include a testbed for studies of slow-light phenomena, variable optical delay lines,[46] clean pulse compression on a chip without pedestal formation by means of the soliton decay mechanism, and soliton-based optical switching and routing with low-energy pulses. Although all of these concepts have been implemented in various geometries and material systems, the SCISSOR system has the potential for providing a highly compact, integrated optical platform for such phenomena. We expect that, as manufacturing techniques continue to improve, microresonator-tailored waveguides such as the SCISSOR system will become important photonic devices.

REFERENCES AND NOTES

1. S. L. McCall, A. F. J. Levi, R. E. Slusher, S. J. Pearton, and R. A. Logan, "Whispering-gallery mode microdisk lasers," Appl. Phys. Lett. **60**, 289–291 (1992).
2. Y. Yamamoto and R. E. Slusher, "Optical Processes in microcavities," Phys. Today **46**(6), 66–74 (1993).
3. J. C. Knight, H. S. T. Driver, R. J. Hutcheon, and G. N. Robertson, "Core-resonance capillary-fiber whispering-gallery-mode laser," Opt. Lett. **17**, 1280–1282 (1992).
4. J. Popp, M. H. Fields, and R. K. Chang, "Q-switching by saturable absorption in microdroplets: elastic scattering and laser emission," Opt. Lett. **22**, 1296–1298 (1997).
5. B. E. Little, S. T. Chu, H. A. Haus, J. Foresi, and J.-P. Laine, "Microring resonator channel dropping filters," J. Lightwave Technol. **15**, 998–1005 (1997).
6. S. Schiller and R. L. Byer, "High-resolution spectroscopy of whispering gallery modes in large dielectric spheres," Opt. Lett. **16**, 1138–1140 (1991).
7. V. V. Vassiliev, V. L. Velichansky, V. S. Ilchenko, M. L. Gorodetsky, L. Hollberg, and A. V. Yarovitsky, "Narrow-line-width diode laser with a high-Q microsphere resonator," Opt. Commun. **158**, 305–312 (1998).
8. C. K. Madsen and G. Lenz, "Optical all-pass filters for phase response design with applications for dispersion compensation," IEEE Photon. Technol. Lett. **10**, 994–996 (1998).
9. V. B. Braginsky, M. L. Gorodetsky, and V. S. Ilchenko, "Quality-factor and nonlinear properties of optical whispering-gallery modes," Phys. Rev. A **137**, 393–397 (1989).
10. F. C. Blom, D. R. van Dijk, H. J. Hoekstra, A. Driessen, and Th. J. A. Popma, "Experimental study of integrated-optics

Fig. 11. Functional dependence of the (a) group-velocity reduction, (b) GVD, (c) third-order dispersion, (d) SPM coefficient, and (e) SS coefficient on the normalized detuning ϕ for a SCISSOR. The parameters have been scaled such that the curves are universal and fit within the same plot limits.

microcavity resonators: toward an all-optical switching device," Appl. Phys. Lett. **71**, 747–749 (1997).

11. D. W. Vernooy, V. S. Ilchenko, H. Mabuchi, E. W. Streed, and H. J. Kimble, "High-*Q* measurements of fused-silica microspheres in the near infrared," Opt. Lett. **23**, 247–249 (1998).

12. V. B. Braginsky and V. S. Ilchenko, "Properties of optical dielectric microresonators," Sov. Phys. Dokl. **32**, 306–307 (1987).

13. We define the finesse as the FSR divided by the full width at half-depth (FWHD) of the resonance peak. Applying this definition to either the phase sensitivity or the intensity buildup, the finesse is calculated as

$$\mathcal{F} = \frac{\text{FSR}}{\text{FWHD}} = \frac{2\pi}{2 \arccos[2r/(1+r^2)]} \xrightarrow[r \approx 1]{} \frac{\pi}{1-r}.$$

14. Implicit in this assumption is that each resonator is not strongly driven; i.e., the transmitted phase shift Φ per resonator is small with respect to unity.

15. G. Lenz, B. J. Eggleton, C. R. Giles, C. K. Madsen, and R. E. Slusher, "Dispersive properties of optical filters for WDM systems," IEEE J. Quantum Electron. **34**, 1390–1402 (1998).

16. For the purpose of quoting the material nonlinearity of standard silica fiber, we have defaulted to a more intuitive definition of the nonlinear coefficient γ such that γPL is the nonlinear phase shift acquired for a power level of P over a distance L.

17. J. E. Heebner and R. W. Boyd, "Enhanced all-optical switching by use of a nonlinear fiber ring resonator," Opt. Lett. **24**, 847–849 (1999).

18. G. P. Agrawal, *Nonlinear Fiber Optics*, 3rd ed. (Academic, San Diego, Calif., 2001).

19. The values of k'_{eff} and γ_{eff} are lowered by factors of 3/4 and 9/16, respectively, from their given maximum values when operating at dispersion extremum points.

20. The simulations used to study pulse evolution in a sequence of waveguide-coupled resonators were carried out by an iterative method in which each iteration consisted of linear and nonlinear phase accumulation during one round trip within the resonator followed by interference at the coupler. Traditional beam or pulse propagation split-step Fourier methods are unnecessary, as structural dispersion possessing a discrete impulse response, is more readily treated in the time domain.

21. Additionally, higher-order dispersive or nonlinear effects render the scattering of solitons inelastic. Under these conditions, the term "solitary wave" is more appropriate.

22. To expand Eq. (18) correctly, the $\mathcal{B}$ term must also be expanded, which will generate more time derivative terms within the square brackets. Thus the SS contribution will consist of not only two $m = 2$ terms but also one $m = 1$ term. For terms such that $m > 1$, the time derivatives implicitly appear to the far left of each term when the square brackets are expanded.

23. H. M. Gibbs, *Optical Bistability: Controlling Light with Light* (Academic, New York, 1985).

24. P. P. Absil, J. V. Hryniewicz, B. E. Little, P. S. Cho, R. A. Wilson, L. G. Jonekis, and P.-T. Ho, "Wavelength conversion in GaAs micro-ring resonators," Opt. Lett. **25**, 554–556 (2000).

25. Y. Xu, R. K. Lee, and A. Yariv, "Propagation and second-harmonic generation of electromagnetic waves in a coupled-resonator optical waveguide," J. Opt. Soc. Am. B **17**, 387–400 (2000).

26. Including the effects of attenuation, the finesse is calculated as

$$\mathcal{F} = \frac{2\pi}{2 \arccos\{2ra/[1+(ra)^2]\}} \xrightarrow[ra \approx 1]{} \frac{\pi}{1-ra},$$

and the transmission is given by

$$T = \frac{a^2 - 2ra \cos\phi + r^2}{1 - 2ra \cos\phi + (ra)^2},$$

where a is the transmission coefficient for a single pass around the resonator. If the attenuation is comparable with the cross coupling, light is resonantly attenuated strongly. Under the condition known as critical coupling ($r = a$), the finesse drops by a factor of 2 and, more important, the transmission drops to zero.

27. M. L. Gorodetsky, A. A. Savchenkov, and V. S. Ilchenko, "Ultimate *Q* of optical microsphere resonators," Opt. Lett. **21**, 453–455 (1996).

28. G. Lenz, J. Zimmermann, T. Katsufuji, M. E. Lines, H. Y. Hwang, S. Spalter, R. E. Slusher, S.-W. Cheong, J. S. Sanghera, and I. D. Aggarwal, "Large Kerr effect in bulk Se-based chalcogenide glasses," Opt. Lett. **25**, 254–256 (2000).

29. B. E. Little and S. T. Chu, "Estimating surface roughness loss and output coupling in microdisk resonators," Opt. Lett. **21**, 1390–1392 (1996).

30. A. Taflove and S. C. Hagness, *Computational Electrodynamics, the Finite-Difference Time-Domain Method* (Artech House, Boston, 2000).

31. S. Blair, J. E. Heebner, and R. W. Boyd, "Beyond the absorption-limited nonlinear phase shift with micro-ring resonators," Opt. Lett. (to be published).

32. W. Chen and D. L. Mills, "Gap solitons and the nonlinear optical response of superlattices," Phys. Rev. Lett. **58**, 160–163 (1987).

33. B. J. Eggleton, R. E. Slusher, C. M. de Sterke, P. A. Krug, and J. E. Sipe, "Bragg grating solitons," Phys. Rev. Lett. **76**, 1627–1630 (1996).

34. A. Yariv, Y. Xu, R. K. Lee, and A. Scherer, "Coupled resonator optical waveguide: a proposal and analysis," Opt. Lett. **24**, 711–713 (1999).

35. B. E. Little, S. T. Chu, J. V. Hryniewicz, and P. P. Absil, "Filter synthesis for periodically coupled microring resonators," Opt. Lett. **25**, 344–346 (2000).

36. S. Pereira, J. E. Sipe, J. E. Heebner, and R. W. Boyd, "Gap solitons in a two-channel side-coupled, integrated, space sequence of resonator structure," Opt. Lett (to be published).

37. M. D. Lukin, M. Fleischhauer, A. S. Zibrov, H. G. Robinson, V. L. Velichansky, L. Hollberg, and M. O. Scully, "Spectroscopy in dense coherent media: line narrowing and interference effects," Phys. Rev. Lett. **79**, 2959–2962 (1997).

38. A. B. Matsko, Y. V. Rostovtsev, H. Z. Cummins, and M. O. Scully, "Using slow light to enhance acousto-optical effects: application to squeezed light," Phys. Rev. Lett. **84**, 5752–5755 (2000).

39. A. B. Matsko, Y. V. Rostovtsev, M. Fleischhauer, and M. O. Scully, "Anomalous stimulated Brillouin scattering via ultraslow light," Phys. Rev. Lett. **86**, 2006–2009 (2001).

40. S. Arnold, C. T. Liu, W. B. Whitten, and J. M. Ramsey, "Room-temperature microparticle-based persistent spectral hole burning memory," Opt. Lett. **16**, 420–422 (1991).

41. N. Dubreuil, J. C. Knight, D. K. Leventhal, V. Sandoghdar, J. Hare, and V. Lefevre, "Eroded monomode optical fiber for whispering-gallery mode excitation in fused-silica microspheres," Opt. Lett. **20**, 813–815 (1995).

42. D. Rafizadeh, J. P. Zhang, S. C. Hagness, A. Taflove, K. A. Stair, S. T. Ho, and R. C. Tiberio, "Waveguide-coupled AlGaAs/GaAs microcavity ring and disk resonators with high finesse and 21.6 nm free-spectral range," Opt. Lett. **22**, 1244 (1997).

43. J.-P. Laine, B. E. Little, and H. A. Haus, "Etch-eroded fiber coupler for whispering-gallery-mode excitation in high-Q silica microspheres," IEEE Photon. Technol. Lett. **11**, 1429–1430 (1999).

44. M. Cai, O. Painter, and K. Vahala, "Observation of critical coupling in a fiber taper to a silica-microsphere whispering-gallery mode system," Phys. Rev. Lett. **85**, 74–77 (2000).

45. B. E. Little and S. T. Chu, "Toward very large-scale integrated photonics," Opt. Photon. News **11**, November 2000, pp. 24–29.

46. G. Lenz, B. J. Eggleton, C. K. Madsen, and R. E. Slusher, "Optical delay lines based on optical filters," IEEE J. Quantum Electron. **37**, 525–532 (2001).